Deformation-dependent effective mobility in Structural Battery Electrolytes

Citation for the original published paper (version of record):
Tu, V., Larsson, F., Runesson, K. et al (2025). Deformation-dependent effective mobility in Structural Battery Electrolytes. International Journal of Solids and Structures, 315. http://dx.doi.org/10.1016/j.ijsolstr.2025.113342

International Journal of Solids and Structures 315 (2025) 113342

Contents lists available at ScienceDirect

International Journal of Solids and Structures

journal homepage: www.elsevier.com/locate/ijsolstr

Deformation-dependent effective mobility in Structural Battery Electrolytes

Vinh Tu [a,b,*], Fredrik Larsson [a], Kenneth Runesson [a], Ralf Jänicke [b]

[a] Department of Industrial and Materials Science, Chalmers University of Technology, SE-41296, Gothenburg, Sweden
[b] Institute of Applied Mechanics, Technische Universität Braunschweig, D-38106, Braunschweig, Germany

ARTICLE INFO

Keywords:
Deformation-dependent mobility
Computational homogenization
Hyperelasticity
Compressible Neo-Hooke
Fickian diffusion
Structural battery electrolyte

ABSTRACT

This paper considers chemical diffusion in a Structural Battery Electrolyte (SBE) under the influence of finite deformation, which serves as a first step towards the more rigorous electro-chemically coupled modeling of deformation-dependent ionic transport in SBEs. The SBE is a porous (bicontinuous) microstructure consisting of a solid (polymer) skeleton, and pores filled with a liquid electrolyte. We present a variationally consistent computational homogenization scheme and exploit 3D-representation of the microstructure to compute the deformation-dependent effective mobility via direct upscaling in a two-step procedure (sequentially coupled approach). The pertinent RVE problem is established for the mechanical (equilibrium) problem under macro-scale deformation control, while adopting Neo-Hooke hyperelasticity for the fine-scale modeling of the solid skeleton. Thereby, the elastic moduli are calibrated based on experimental data for the effective response. Subsequently, Fickian diffusion, with a constant mobility in the liquid electrolyte is considered in the deformed pore space. Exploiting a pull-back to the reference configuration, we avoid remeshing while still incorporating the necessary pore space deformation. By adopting a suitable constitutive model for the fictitious solid in the pore space, we also prevent self-penetration of the solid skeleton during deformation, which mimics contact behavior without explicitly solving a computationally expensive contact problem involving contact search. Upon homogenizing the local ionic flux, we obtain the effective mobility pertaining to the macro-scale chemical potential gradient, while noting that the RVE-problem is linear in the chemical potential for a given macro-scale deformation gradient. The numerical results show that when the macro-scale loading is of compressive type, the pore volume is reduced and, as a direct consequence, the effective mobility becomes smaller. In essence, the framework can track the geometrically induced anisotropy of the RVE under mechanical loading, corresponding to a change in the computational domain for the transport problem, thereby influencing the ionic flux. E.g. for a bicontinuous SBE with 37% initial porosity and an externally applied macroscopic compression of 20% strain, we could observe up to 26% reduction in the effective mobility components.

1. Introduction

The structural battery is a multifunctional material with the ability to carry mechanical loads, while simultaneously storing and releasing energy (Asp and Greenhalgh, 2014; Asp et al., 2019). Conventional batteries often use liquid electrolytes for ion transfer between electrodes. In contrast, the structural battery employs a Structural Battery Electrolyte (SBE), which comprises two continuous phases: a liquid electrolyte and an interconnected solid (polymer) skeleton. The liquid electrolyte facilitates ion transfer, while the solid polymer phase provides structural integrity (Shirshova et al., 2013; Ihrner et al., 2017; Schneider et al., 2019). The aim is to make each component of the structural battery multifunctional and with optimized performance to ensure significant weight and volume savings (Asp and Greenhalgh, 2014; Asp et al., 2019; Johannisson et al., 2019). However, the complexity of the structural battery introduces numerous challenges that must be addressed. While some modeling efforts have been conducted on the SBE (Tu et al., 2023; Carlstedt et al., 2022), the field remains relatively new, indicating a substantial need for further research.

This paper aims to develop a framework for simulating deformation-dependent diffusion in a SBE. Given that structural batteries are subjected to mechanical loads, it is crucial to evaluate the extent to which these loads adversely impact the diffusion within the battery. Outside the realm of (structural) batteries, the topic of deformation-dependent diffusion has been explored within the porous media and composite research communities.

Klepach and Zohdi (2014) formulated a diffusivity tensor that depends on the volumetric strain via $J = \det(\boldsymbol{F})$. For elasticity, they employed a Kirchhoff–Saint Venant material. Voges et al. (2022) compared the assumption of isotropy of the mobility tensor in (i) the current

* Corresponding author at: Department of Industrial and Materials Science, Chalmers University of Technology, SE-41296, Gothenburg, Sweden.
E-mail address: vinh.tu@chalmers.se (V. Tu).

https://doi.org/10.1016/j.ijsolstr.2025.113342
Received 2 November 2024; Received in revised form 21 February 2025; Accepted 12 March 2025
Available online 28 March 2025

configuration vs. (ii) the reference configuration. Their conclusion was that the assumption of isotropy has a significant effect on the final results. It was also noted that this topic is poorly documented in the literature. Griffiths et al. (2020) looked at nanoporous metal based composites in a chemo-electro-mechanical framework based on small strains. However, they note that the classic Poisson–Nernst–Planck framework fails to account for certain transport limiting effects such as the spatial effects of the ions. Therefore, they introduce an enhanced Poisson–Nernst–Planck theory to produce a more physically appropriate ion transport response. Griso and Rohan (2007), Rohan and Cimrman (2012) worked on homogenization of a diffusion–deformation problem where they accounted a sub-microscopic scale where the solid and fluid parts are distinguishable. Here, they evaluated homogenized coefficients by exploiting the asymptotic homogenization procedure.

Attempts to establish more general chemo-mechanical couplings based on computational homogenization are those of Kaessmair and Steinmann (2018), and Polukhov and Keip (2020), who provide numerical examples for generic microstructural designs. Another recent example is the work by Waseem et al. (2020) who treat multi-scale transient diffusion coupled to mechanics.

The novelty of this paper lies in the formulation of a variationally consistent computational homogenization scheme for transport in the pore space of a bicontinuous medium under large deformations, including Direct Numerical Upscaling of the effective ionic mobility, providing a complete multiscale framework for the deformation-dependent effective mobility. In other words, we will conduct a virtual material test of a microstructure to compute how the effective (homogenized) mobility changes with deformation. Here, we propose a sequentially coupled approach to transport in a deformed pore space under large deformations. A Representative Volume Element (RVE) will be used to represent the SBE microstructure, whereby the artificial RVE is of the so-called "trabecular" type, generated according to Tu et al. (2020). We consider finite strains and employ a compressible Neo-Hooke material model for the solid skeleton. Subsequently, we assume diffusion with a Fickian constitutive relation and a constant mobility in the deformed configuration. Note that we introduce a fictitious solid material in the pore space domain to track the pore space deformation, which is necessary for solving the transport problem in the deformed pore space domain. Exploiting a pull-back to the reference configuration, we avoid remeshing while still incorporating the necessary pore space deformation. Further, by adopting a suitable constitutive model in the fictitious solid in the pore space, we also prevent self-penetration of the solid skeleton during deformation, which mimics contact behavior without explicitly solving a computationally expensive contact problem involving contact search. In short, this framework accounts for deformation by establishing the deformation-dependent Piola-flux (in the undeformed configuration). Indeed, it is the electro-chemical ionic transport that is relevant to SBEs. However, investigating the deformation-dependent diffusion will serve as a first step towards the more rigorous electro-chemically coupled modeling of deformation-dependent ionic transport in SBEs.

The paper is organized as follows: Section 2 describes the governing equations, comprising the structural analysis problem and the diffusion equation along with their constitutive relations. In Section 3, we establish the foundational framework for computational homogenization to formulate a RVE problem. Section 4 elaborates on the numerical implementation specifics and presents the simulation results. Finally, Section 5 concludes the paper with a brief discussion and a perspective on potential future improvements.

2. Governing equations

This section provides an overview of the governing equations used to simulate deformation-dependent diffusion. The relevant constitutive relations are also defined. The SBE microstructure under consideration is a porous bicontinuous electrolyte material. It consists of a continuous liquid electrolyte domain Ω_{E}, and a distinct continuous solid skeleton (polymer) domain Ω_{S}. The union of these domains results in the full domain $\Omega = \Omega_{\mathrm{S}} \cup \Omega_{\mathrm{E}}$. Furthermore, we define the interface $\Gamma_{\mathrm{S/E}} = \partial\Omega_{\mathrm{S}} \cap \partial\Omega_{\mathrm{E}}$. This split is introduced to address the distinct physical phenomena operating within separate domains. See Fig. 1 for the domain and boundary decompositions.

2.1. Balance equations for the fine-scale problem

When the SBE microstructure is subjected to mechanical loads, the solid skeleton is deformed according to the mapping $\boldsymbol{\varphi}$: $\Omega \to \omega$, where $\omega = \omega_{\mathrm{S}} \cup \omega_{\mathrm{E}}$. More precisely, we consider the deformation at point $\boldsymbol{X} \in \Omega$ to $\boldsymbol{x} \in \omega$ with $\boldsymbol{x} = \boldsymbol{\varphi}(\boldsymbol{X}) = \boldsymbol{X} + \boldsymbol{u}(\boldsymbol{X})$, where $\boldsymbol{u}(\boldsymbol{X})$ is the displacement field. The mechanical problem reads: Find $\boldsymbol{u} : \Omega \to \mathbb{R}^3$ that solves the equilibrium equation with boundary conditions

$$-\boldsymbol{P} \cdot \boldsymbol{\nabla}_X = \boldsymbol{0} \quad \text{in } \Omega, \tag{1a}$$

$$\boldsymbol{u} = \boldsymbol{u}^{\mathrm{p}} \quad \text{on } \Gamma_{\mathrm{D}}^{(u)}, \tag{1b}$$

$$\boldsymbol{t}_X = \boldsymbol{P} \cdot \boldsymbol{N} = \boldsymbol{t}_X^{\mathrm{p}} \quad \text{on } \Gamma_{\mathrm{N}}^{(u)}, \tag{1c}$$

which represents a solvable system when complemented with the constitutive relations defined below. Here, $\boldsymbol{P}$ is the 1st Piola–Kirchhoff stress tensor. The equilibrium equation is valid on the entire domain $\Omega = \Omega_{\mathrm{S}} \cup \Omega_{\mathrm{E}}$, and the boundary conditions are exemplified on $\partial\Omega = \Gamma_{\mathrm{D}}^{(u)} \cup \Gamma_{\mathrm{N}}^{(u)}$ in terms of Dirichlet (1b) and Neumann conditions (1c).

In this paper, it is assumed that the SBE is drained during mechanical loading. For the case of a drained (open-ended) SBE, the liquid inside the microstructure pores is allowed to freely redistribute (macroscopically) without any resistance. Another viable assumption is the case of an undrained (closed-ended) SBE, where the liquid is instead assumed to be trapped inside the microstructure pores. In that case, an externally applied mechanical loading results in an increase of the internal liquid pressure. Consequently, a higher effective mechanical stiffness is achieved due to the additional bulk modulus contribution from the trapped liquid. In reality, the SBE most likely has a behavior that lies somewhere in-between the two extreme assumptions, i.e. partially drained. The drained assumption is chosen here for simplicity since it decouples the liquid from the mechanical response.

In order to compute the deformation-dependent mobility via a diffusion problem in undeformed configuration, it is crucial to know how much the pore space deforms. This can be achieved by assigning a small fictitious stiffness to the liquid electrolyte domain Ω_{E}, whereby mechanically loading the microstructure will lead to deformations in Ω_{E} without introducing any significant reaction forces acting on Ω_{S}. Additionally, we also do this as a way to avoid self-penetration of the solid phase by requiring the volume of the locally deformed pore space to be strictly positive.

The next step is to analyze the diffusion. Mass balance, in the deformed format, for a single diffusing species in the deformed pore space $\omega_{\mathrm{E}} = \boldsymbol{\varphi}(\Omega_{\mathrm{E}})$ reads

$$\boldsymbol{j} \cdot \boldsymbol{\nabla} = 0 \quad \text{in } \omega_{\mathrm{E}}. \tag{2}$$

Next, performing pull-back, the material format leads to the following problem: Find the chemical potential $\mu : \Omega_{\mathrm{E}} \to \mathbb{R}$, that solves the system

$$\boldsymbol{J} \cdot \boldsymbol{\nabla}_X = 0 \quad \text{in } \Omega_{\mathrm{E}}. \tag{3a}$$

$$\mu = \mu^{\mathrm{p}} \quad \text{on } \Gamma_{\mathrm{D}}^{(\mu)}, \tag{3b}$$

$$J_N := \boldsymbol{J} \cdot \boldsymbol{N} = J^{\mathrm{p}} \quad \text{on } \Gamma_{\mathrm{N}}^{(\mu)}, \tag{3c}$$

$$J_N = 0 \quad \text{on } \Gamma_{\mathrm{S/E}}, \tag{3d}$$

which is solvable when complemented with the constitutive relations defined below. In (3a), we introduced the molar mass flux $\boldsymbol{J} = J\boldsymbol{F}^{-1} \cdot \boldsymbol{j}$ in the undeformed configuration. Here, $\boldsymbol{F} = \boldsymbol{\varphi} \otimes \boldsymbol{\nabla}_X = \boldsymbol{I} + \boldsymbol{u} \otimes \boldsymbol{\nabla}_X$ is the deformation gradient, and $J = \det(\boldsymbol{F})$ is the relative volume

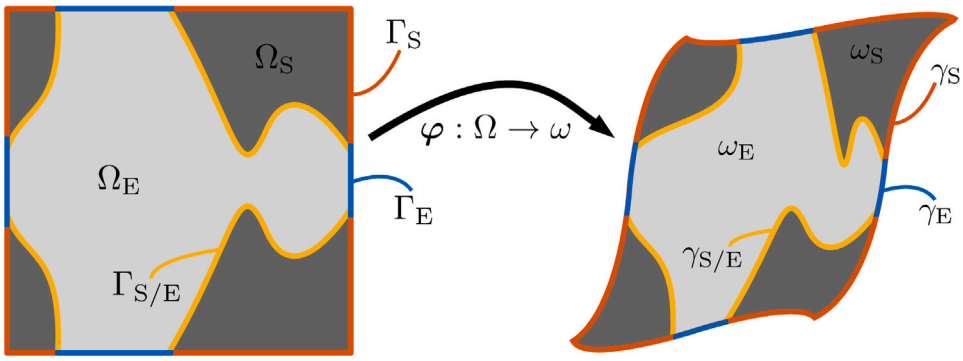

Fig. 1. The SBE consists of solid and electrolyte domains, $\Omega = \Omega_S \cup \Omega_E$. The entire external boundary of the SBE is decomposed as $\partial\Omega = \Gamma_S \cup \Gamma_E = \Gamma_D^{(\varphi)} \cup \Gamma_N^{(\varphi)}$, and the boundary surrounding the electrolyte domain is decomposed as $\partial\Omega_E = \Gamma_E \cup \Gamma_{S/E} = \Gamma_{D,\alpha}^{(\mu)} \cup \Gamma_{N,\alpha}^{(\mu)} \cup \Gamma_{S/E}$. A 2D RVE is used in the illustration for simplicity, even though the framework primarily applies to 3D RVEs. The same decomposition is analogously applied on the deformed domain ω; this is left out for brevity.

change. The diffusion process inside the solid domain Ω_S is assumed to be negligible; hence, the system (3) is valid only in the electrolyte domain Ω_E, whose boundary is decomposed as $\partial\Omega_E = \Gamma_D^{(\mu)} \cup \Gamma_N^{(\mu)} \cup \Gamma_{S/E}$. Additionally, (3d) is used to prohibit ion transport through the solid-electrolyte interface $\Gamma_{S/E} = \partial\Omega_S \cap \partial\Omega_E$. Lastly, (3b) and (3c) are examples of the external boundary conditions of the Dirichlet and the Neumann type, respectively.

2.2. Constitutive relations of the fine-scale model

Neo-Hooke hyperelasticity is assumed for the fine-scale modeling of the solid skeleton. There are multiple variants of the Neo-Hooke material model. In this paper, a compressible version is adopted (Bonet and Wood, 2008). The volume specific strain energy density Ψ reads as follows

$$\Psi(\boldsymbol{C}) = \frac{G}{2}\,[\mathrm{tr}(\boldsymbol{C}) - 3] - G\ln(J) + \frac{\lambda}{2}\ln(J)^2, \tag{4}$$

where λ and G are the elastic Lamé parameters. Further, $\boldsymbol{C} = \boldsymbol{F}^T \cdot \boldsymbol{F}$ is the right Cauchy–Green deformation tensor, and we identify $J = \sqrt{\det(\boldsymbol{C})}$. The 1st Piola–Kirchhoff stress is expressed as an explicit function of the deformation gradient: $\boldsymbol{P} = 2\boldsymbol{F} \cdot \frac{\partial \Psi}{\partial \boldsymbol{C}}$.

As previously mentioned, we need to model the liquid using a fictitious stiffness in order to define a map $\boldsymbol{\varphi}$ also on Ω_E. Hence, assuming Neo-Hooke hyperelasticity also in the liquid domain, we state the stress for both domains as

$$\boldsymbol{P}(\boldsymbol{F}) = \begin{cases} \boldsymbol{P}_S(\boldsymbol{F}) & \text{in } \Omega_S, \\ \boldsymbol{P}_E(\boldsymbol{F}) & \text{in } \Omega_E, \end{cases} \tag{5}$$

where $\boldsymbol{P}_S(\boldsymbol{F})$ is the constitutive model for the solid skeleton, and $\boldsymbol{P}_E(\boldsymbol{F})$ is the fictitious elastic model of the electrolyte pore space. Note that for any finite value of λ, the Neo-Hooke model in (4) will enforce $J > 0$. Hence, even for a small fictitious stiffness, the pore space will prevent penetration of the solid constituents.

For diffusion, we assume a Fickian constitutive relation and a constant mobility. In the deformed configuration, the constitutive model reads

$$\boldsymbol{j} = -\boldsymbol{m} \cdot \boldsymbol{g}, \quad \boldsymbol{g} := \nabla\mu, \tag{6}$$

where $\boldsymbol{m}$ is the intrinsic fine-scale mobility tensor[1] of the considered ionic species. A pull-back to the undeformed configuration gives the Piola-flux

$$\boldsymbol{J}(\boldsymbol{F}, \boldsymbol{G}) = -\boldsymbol{M}(\boldsymbol{F}) \cdot \boldsymbol{G}, \quad \boldsymbol{G} := \boldsymbol{F}^T \cdot \boldsymbol{g} = \nabla_X \mu, \tag{7}$$

with

$$\boldsymbol{M}(\boldsymbol{F}) = J\boldsymbol{F}^{-1} \cdot \boldsymbol{m} \cdot \boldsymbol{F}^{-T}, \tag{8}$$

representing the local deformation-dependent[2] mobility in undeformed configuration. The above relations are obtained upon using the Piola-identity $[J\boldsymbol{F}^{-T}] \cdot \nabla_X = \boldsymbol{0}$.

2.3. Weak format of the fine-scale problem

The standard space-variational format corresponding to (1) and (3) reads: Find $\boldsymbol{u} \in \mathbb{U}$ and $\mu \in \mathbb{M}$ in the appropriately defined spaces that solve

$$\int_\Omega [\delta\boldsymbol{u} \otimes \nabla_X] : \boldsymbol{P}(\boldsymbol{F})\,\mathrm{d}\Omega = \int_{\Gamma_N^{(u)}} \boldsymbol{t}_X^P \cdot \delta\boldsymbol{u}\,\mathrm{d}\Gamma \quad \forall \delta\boldsymbol{u} \in \mathbb{U}^0, \tag{9a}$$

$$-\int_{\Omega_E} \nabla_X \delta\mu \cdot \boldsymbol{J}(\boldsymbol{F}, \boldsymbol{G})\,\mathrm{d}\Omega = -\int_{\Gamma_N^{(\mu)}} \delta\mu\, J^P\,\mathrm{d}\Gamma \quad \forall \delta\mu \in \mathbb{M}^0, \tag{9b}$$

where $\mathbb{U}^0$ and $\mathbb{M}^0$ are the appropriately defined test spaces.

3. Two-scale model of deformation-dependent diffusion

Virtual material testing can be performed on heterogeneous microstructures to derive the relevant effective material properties that characterize the material response on the macro-scale. Here, we employ Computational Homogenization, where the heterogeneous microstructure of the SBE is represented by an RVE in 3D that occupies the domain $\Omega_\square$. The finite element method is then used to solve the RVE problem, see e.g. Miehe et al. (1999), Miehe and Koch (2002), Kouznetsova et al. (2001), Geers et al. (2010) and Yvonnet. The RVE is chosen as a repeating unit-cell, which motivates the choice of periodic boundary conditions (Michel et al., 1999). For closely related approaches (classical homogenization methods), see the works by Hill (1963), Zohdi and Wriggers (2008), and Nemat-Nasser and Hori (2013) on mean-field and homogenization theories.

3.1. First order homogenization — Preliminaries

In this paper, the main focus will be on studying the RVE on the sub-scale level. Information of the macro-scale solution is sent to the sub-scale in a prolongation step; it serves as the loading data to the RVE problem. After solving the RVE problem, effective properties and effective fluxes can be computed via homogenization.

[1] Here, the intrinsic mobility $\boldsymbol{m}$ is the mobility of pure liquid electrolyte. This is usually a property that is given by the manufacturer and supplier. In the case that this information is missing, it can easily be measured. Therefore, in this paper, the intrinsic mobility $\boldsymbol{m}$ is treated as a known property.

[2] Here, "local deformation-dependent" should be interpreted as the pertinent mobility for analysis on the undeformed domain Ω_E.

The first step is to define the RVE volume averaging operators and the initial porosity ϕ_0 as

$$\langle \bullet \rangle_{\square} := \frac{1}{|\Omega_{\square}|} \int_{\Omega_{\square}} \bullet \, \mathrm{d}\Omega, \tag{10a}$$

$$\langle \bullet \rangle_{\square,\mathrm{E}} := \frac{1}{|\Omega_{\square,\mathrm{E}}|} \int_{\Omega_{\square,\mathrm{E}}} \bullet \, \mathrm{d}\Omega, \tag{10b}$$

$$\phi_0 := \frac{|\Omega_{\square,\mathrm{E}}|}{|\Omega_{\square}|}. \tag{10c}$$

In the second step, we define the standard prolongation[3] rules as follows

$$\boldsymbol{u} = \boldsymbol{u}^{\mathrm{M}}[\bar{\boldsymbol{u}}] + \boldsymbol{u}^{\mathrm{S}}, \tag{11a}$$

$$\mu = \mu^{\mathrm{M}}[\bar{\mu}] + \mu^{\mathrm{S}}, \tag{11b}$$

where

$$\boldsymbol{u}^{\mathrm{M}}[\bar{\boldsymbol{u}}](\bar{\boldsymbol{X}};\boldsymbol{X}) := \bar{\boldsymbol{u}}(\bar{\boldsymbol{X}}) + \bar{\boldsymbol{H}}[\bar{\boldsymbol{u}}](\bar{\boldsymbol{X}}) \cdot [\boldsymbol{X} - \bar{\boldsymbol{X}}], \quad \bar{\boldsymbol{H}} := \bar{\boldsymbol{u}} \otimes \boldsymbol{\nabla}_X = \bar{\boldsymbol{F}} - \boldsymbol{I}, \tag{12a}$$

$$\mu^{\mathrm{M}}[\bar{\mu}](\bar{\boldsymbol{X}};\boldsymbol{X}) := \bar{\mu}(\bar{\boldsymbol{X}}) + \bar{\boldsymbol{G}}[\bar{\mu}](\bar{\boldsymbol{X}}) \cdot [\boldsymbol{X} - \bar{\boldsymbol{X}}], \quad \bar{\boldsymbol{G}} := \boldsymbol{\nabla}_X \bar{\mu}. \tag{12b}$$

Here, the sub-scale fields $\boldsymbol{u}$ and μ are decomposed into macro-scale parts, $\boldsymbol{u}^{\mathrm{M}}$ and μ^{M}, and micro-scale/fluctuating parts, $\boldsymbol{u}^{\mathrm{S}}$ and μ^{S}. The homogenized fields $\bar{\boldsymbol{u}}(\bar{\boldsymbol{X}})$ and $\bar{\mu}(\bar{\boldsymbol{X}})$ are the smooth macro-scale solutions pertaining to the smooth macro-scale domain $\bar{\Omega}$. The macro-scale parts $\boldsymbol{u}^{\mathrm{M}}(\boldsymbol{X})$ and $\mu^{\mathrm{M}}(\boldsymbol{X})$ are the constructed (first-order) Taylor expansions that live in the RVE domain $\Omega_{\square}$ to represent the fully resolved fine-scale fields.

3.2. Macro-scale problem

There are multiple computational homogenization strategies; one viable choice is the framework of Variationally Consistent Homogenization (Larsson et al., 2010; Bharali et al., 2021; Börjesson et al., 2023; Rollin et al., 2023). Following this framework, we formulate the weak form of the macro-scale problem as follows: Find $\bar{\boldsymbol{u}} \in \bar{\mathbb{U}}$ and $\bar{\mu} \in \bar{\mathbb{U}} \times \bar{\mathbb{M}}$ that solve[4]

$$\int_{\bar{\Omega}} [\delta\bar{\boldsymbol{u}} \otimes \boldsymbol{\nabla}_X] : \bar{\boldsymbol{P}}\{\bar{\boldsymbol{F}}\} \, \mathrm{d}\Omega = \int_{\bar{\Gamma}_{\mathrm{N}}^{(u)}} \bar{\boldsymbol{t}}_X^{\mathrm{P}} \cdot \delta\bar{\boldsymbol{u}} \, \mathrm{d}\Gamma \quad \forall \delta\bar{\boldsymbol{u}} \in \bar{\mathbb{U}}^0, \tag{13a}$$

$$-\int_{\bar{\Omega}} \boldsymbol{\nabla}_X \delta\bar{\mu} \cdot \bar{\boldsymbol{J}}\{\bar{\boldsymbol{F}},\bar{\boldsymbol{G}}\} \, \mathrm{d}\Omega = -\int_{\bar{\Gamma}_{\mathrm{N}}^{(\mu)}} \delta\bar{\mu} \, \bar{J}^{\mathrm{P}} \, \mathrm{d}\Gamma \quad \forall \delta\bar{\mu} \in \bar{\mathbb{M}}^0. \tag{13b}$$

where $\bar{\boldsymbol{t}}_X^{\mathrm{P}}$ and $\bar{J}^{\mathrm{P}}$ are suitably defined macroscopic loading data. The homogenized constitutive quantities are defined as

$$\bar{\boldsymbol{P}} = \langle \boldsymbol{P} \rangle_{\square}, \tag{14a}$$

$$\bar{\boldsymbol{J}} = \phi_0 \langle \boldsymbol{J} \rangle_{\square,\mathrm{E}}, \tag{14b}$$

and become implicit functions of $\bar{\boldsymbol{F}}$ and $\bar{\boldsymbol{G}}$ through the RVE problem, see Section 3.3. Here, we note that (13a) pertaining to drained elastic response is independent of $\bar{\mu}$, while (13b) allows for the solution of $\bar{\mu}$ for known solution $\bar{\boldsymbol{u}}$ of (13a).

Localizing (13), we identify the strong format on macro-scale as

$$-\bar{\boldsymbol{P}} \cdot \boldsymbol{\nabla}_X = 0 \quad \text{in } \bar{\Omega}, \tag{15a}$$

$$\bar{\boldsymbol{J}} \cdot \boldsymbol{\nabla}_X = 0 \quad \text{in } \bar{\Omega}, \tag{15b}$$

$$\bar{\boldsymbol{u}} = \bar{\boldsymbol{u}}^{\mathrm{P}} \quad \text{on } \bar{\Gamma}_{\mathrm{D}}^{(u)}, \tag{15c}$$

$$\bar{\boldsymbol{P}} \cdot \boldsymbol{N} = \bar{\boldsymbol{t}}_X^{\mathrm{P}} \quad \text{on } \bar{\Gamma}_{\mathrm{N}}^{(u)}, \tag{15d}$$

$$\bar{\mu} = \bar{\mu}^{\mathrm{P}} \quad \text{on } \bar{\Gamma}_{\mathrm{D}}^{(\mu)}, \tag{15e}$$

$$\bar{\boldsymbol{J}} \cdot \boldsymbol{N} = \bar{J}^{\mathrm{P}} \quad \text{on } \bar{\Gamma}_{\mathrm{N}}^{(\mu)}, \tag{15f}$$

where $\bar{\Omega}$ is the total domain, now considered as an effective mixture. The boundary is decomposed into $\partial\bar{\Omega} = \bar{\Gamma}_{\mathrm{D}}^{(u)} \cup \bar{\Gamma}_{\mathrm{N}}^{(u)} = \bar{\Gamma}_{\mathrm{D}}^{(\mu)} \cup \bar{\Gamma}_{\mathrm{N}}^{(\mu)}$ based on the effective Dirichlet $(\bar{\boldsymbol{u}}^{\mathrm{P}}, \bar{\mu}^{\mathrm{P}})$ and Neumann boundary condition $(\bar{\boldsymbol{t}}_X^{\mathrm{P}}, \bar{\boldsymbol{J}}^{\mathrm{P}})$. The corresponding deformation map is $\bar{\boldsymbol{\varphi}} : \bar{\Omega} \to \bar{\omega}$, where $\bar{\boldsymbol{\varphi}}(\bar{\boldsymbol{X}}) = \bar{\boldsymbol{X}} + \bar{\boldsymbol{u}}(\bar{\boldsymbol{X}})$.

3.3. RVE problems for equilibrium and mass balance of diffusing species

The strategy for this RVE problem is to solve for the equilibrium and the diffusion equations sequentially. First, we solve for $\boldsymbol{u}\{\bar{\boldsymbol{F}}\}$ from the equilibrium equation to obtain $\boldsymbol{F} = \boldsymbol{F}\{\bar{\boldsymbol{F}}\} = \boldsymbol{I} + \boldsymbol{u}\{\bar{\boldsymbol{F}}\} \otimes \boldsymbol{\nabla}_X$. In the second step, we use the local deformation gradient $\boldsymbol{F} = \boldsymbol{F}\{\bar{\boldsymbol{F}}\}$ in the RVE to solve for $\mu = \mu\{\bar{\boldsymbol{F}}, \bar{\boldsymbol{G}}\}$ from the diffusion equation.

The weak form of the RVE problem is formulated as follows:

(i) For given $\bar{\boldsymbol{F}}$, find $\boldsymbol{u}\{\bar{\boldsymbol{F}}\} = \boldsymbol{u} \in \mathbb{U}_{\square}$ and $(\lambda, \bar{\lambda}) \in \mathbb{L}_{\square}^{u} \times \mathbb{R}^3$ that solve

$$\frac{1}{|\Omega_{\square}|} \int_{\Omega_{\square}} \boldsymbol{P}(\boldsymbol{I} + \boldsymbol{u} \otimes \boldsymbol{\nabla}_X) : [\delta\boldsymbol{u} \otimes \boldsymbol{\nabla}_X] \, \mathrm{d}\Omega - \frac{1}{|\Omega_{\square}|} \int_{\Gamma_{\square}^{+}} \lambda \cdot [\![\delta\boldsymbol{u}]\!]_{\square} \, \mathrm{d}\Gamma - \bar{\lambda} \cdot \left[\frac{1}{|\Omega_{\square}|} \int_{\Omega_{\square}} \delta\boldsymbol{u} \, \mathrm{d}\Omega \right] = 0 \quad \forall \delta\boldsymbol{u} \in \mathbb{U}_{\square}, \tag{16a}$$

$$-\frac{1}{|\Omega_{\square}|} \int_{\Gamma_{\square}^{+}} \delta\lambda \cdot [\![\boldsymbol{u}]\!]_{\square} \, \mathrm{d}\Gamma = -\frac{1}{|\Omega_{\square}|} \int_{\Gamma_{\square}^{+}} \delta\lambda \otimes [\![\boldsymbol{X}]\!]_{\square} \, \mathrm{d}\Gamma : [\bar{\boldsymbol{F}} - \boldsymbol{I}] \quad \forall \delta\lambda \in \mathbb{L}_{\square}^{u}, \tag{16b}$$

$$-\delta\bar{\lambda} \cdot \left[\frac{1}{|\Omega_{\square}|} \int_{\Omega_{\square}} \boldsymbol{u} \, \mathrm{d}\Omega \right] = 0 \quad \forall \delta\bar{\lambda} \in \mathbb{R}^3. \tag{16c}$$

(ii) For given local deformation gradient $\boldsymbol{F}\{\bar{\boldsymbol{F}}\}$ and $\bar{\boldsymbol{G}}$, find $\mu\{\bar{\boldsymbol{F}}, \bar{\boldsymbol{G}}\} = \mu \in \mathbb{M}_{\square}$ and $(\lambda, \bar{\lambda}) \in \mathbb{L}_{\square}^{\mu} \times \mathbb{R}$ that solve

$$-\frac{1}{|\Omega_{\square}|} \int_{\Omega_{\square,\mathrm{E}}} \boldsymbol{J}(\boldsymbol{F}\{\bar{\boldsymbol{F}}\}, \boldsymbol{G}) \cdot [\boldsymbol{\nabla}_X \delta\mu] \, \mathrm{d}\Omega + \frac{1}{|\Omega_{\square}|} \int_{\Gamma_{\square,\mathrm{E}}^{+}} \lambda \, [\![\delta\mu]\!]_{\square} \, \mathrm{d}\Gamma - \bar{\lambda} \cdot \left[\frac{1}{|\Omega_{\square}|} \int_{\Omega_{\square,\mathrm{E}}} \delta\mu \, \mathrm{d}\Omega \right] = 0 \quad \forall \delta\mu \in \mathbb{M}_{\square}, \tag{17a}$$

$$\frac{1}{|\Omega_{\square}|} \int_{\Gamma_{\square,\mathrm{E}}^{+}} \delta\lambda \, [\![\mu]\!]_{\square} \, \mathrm{d}\Gamma = \frac{1}{|\Omega_{\square}|} \int_{\Gamma_{\square,\mathrm{E}}^{+}} \delta\lambda \, [\![\boldsymbol{X}]\!]_{\square} \, \mathrm{d}\Gamma \cdot \bar{\boldsymbol{G}} \quad \forall \delta\lambda \in \mathbb{L}_{\square}^{\mu}, \tag{17b}$$

$$-\delta\bar{\lambda} \cdot \left[\frac{1}{|\Omega_{\square}|} \int_{\Omega_{\square,\mathrm{E}}} \mu \, \mathrm{d}\Omega \right] = 0 \quad \forall \delta\bar{\lambda} \in \mathbb{R}. \tag{17c}$$

Remark. The diffusion problem is linear in $(\mu, \lambda, \hat{\lambda})$ for any given value of $\bar{\boldsymbol{F}}$.

Here, the Lagrange multipliers $\delta\lambda \in \mathbb{L}_{\square}^{u}$ and $\delta\lambda \in \mathbb{L}_{\square}^{\mu}$ enforce weakly periodic boundary conditions, while $\delta\bar{\lambda} \in \mathbb{R}^3$ and $\delta\bar{\lambda} \in \mathbb{R}$ represent the scale linking to prevent rigid body motion. Additionally, the difference operator $[\![\bullet]\!]_{\square}(\boldsymbol{x}) := \bullet(\boldsymbol{x}) - \bullet(\boldsymbol{x}^{-}(\boldsymbol{x}))$ is introduced when enforcing weakly periodic boundary conditions (WPBC), cf. Larsson et al. (2011). In this context, $\boldsymbol{x} \in \Gamma_{\square}^{+}$ represents an image point, while $\boldsymbol{x}^{-}(\boldsymbol{x}) \in \Gamma^{-} = \Gamma_{\square} \setminus \Gamma_{\square}^{+}$ is the corresponding mirror point.

In order to compute the macro-scale mobility $\bar{\boldsymbol{M}}$ in the relation

$$\bar{\boldsymbol{J}}\{\bar{\boldsymbol{F}}, \bar{\boldsymbol{G}}\} = -\bar{\boldsymbol{M}}\{\bar{\boldsymbol{F}}\} \cdot \bar{\boldsymbol{G}}, \tag{18}$$

[3] Kouznetsova et al. (2004) has proposed a higher-order approach.

[4] Here, the $\{\bullet\}$ notation is introduced to denote implicit dependence.

we proceed as follows: Firstly, we note that the local flux can be (re)written as

$$\boldsymbol{J}\{\bar{\boldsymbol{F}},\bar{\boldsymbol{G}}\} = -\boldsymbol{M}(\boldsymbol{F}\{\bar{\boldsymbol{F}}\})\cdot[\bar{\boldsymbol{G}}+\boldsymbol{\nabla}_X\mu^{\mathrm{S}}], \tag{19}$$

where we used that

$$\boldsymbol{\nabla}_X\mu = \boldsymbol{\nabla}_X\mu^{\mathrm{M}} + \boldsymbol{\nabla}_X\mu^{\mathrm{S}} = \bar{\boldsymbol{G}} + \boldsymbol{\nabla}_X\mu^{\mathrm{S}}. \tag{20}$$

As a consequence, we rewrite the diffusion problem as that of finding $\mu^{\mathrm{S}} \in \mathbb{M}_{\square}$

$$\begin{aligned}
&\frac{1}{|\Omega_{\square}|}\int_{\Omega_{\square,\mathrm{E}}} \boldsymbol{\nabla}_X\delta\mu\cdot\boldsymbol{M}\cdot\boldsymbol{\nabla}_X\mu^{\mathrm{S}}\,\mathrm{d}\Omega + \frac{1}{|\Omega_{\square}|}\int_{\Gamma^+_{\square,\mathrm{E}}} [\![\delta\mu]\!]_{\square}\,\lambda\,\mathrm{d}\Gamma \\
&+\left[\frac{1}{|\Omega_{\square}|}\int_{\Omega_{\square,\mathrm{E}}}\delta\mu\,\mathrm{d}\Omega\right]\bar{\lambda} = -\left[\frac{1}{|\Omega_{\square}|}\int_{\Omega_{\square,\mathrm{E}}}\boldsymbol{\nabla}_X\delta\mu\cdot\boldsymbol{M}\,\mathrm{d}\Omega\right]\cdot\bar{\boldsymbol{G}} \\
&\qquad\qquad \forall\delta\mu\in\mathbb{M}_{\square}, \qquad (21a)\\
&\frac{1}{|\Omega_{\square}|}\int_{\Gamma^+_{\square,\mathrm{E}}}\delta\lambda\,[\![\mu^{\mathrm{S}}]\!]_{\square}\,\mathrm{d}\Gamma = 0 \\
&\qquad\qquad \forall\delta\lambda\in\mathbb{L}^{\mu}_{\square}, \qquad (21b)\\
&\delta\bar{\lambda}\cdot\left[\frac{1}{|\Omega_{\square}|}\int_{\Omega_{\square,\mathrm{E}}}\mu^{\mathrm{S}}\,\mathrm{d}\Omega\right] = 0 \\
&\qquad\qquad \forall\delta\bar{\lambda}\in\mathbb{R}. \qquad (21c)
\end{aligned}$$

For a fixed (given) value of $\bar{\boldsymbol{F}}$, we thus realize that the linearity of the diffusion problem allows for the expansion

$$\mu^{\mathrm{S}}\{\bar{\boldsymbol{F}},\bar{\boldsymbol{G}}\} = \sum_{k=1}^{3}\hat{\mu}^{(k)}\{\bar{\boldsymbol{F}}\}\,\bar{G}_k, \tag{22}$$

in terms of sensitivity fields $\hat{\mu}^{(k)}$ for each Cartesian component $\bar{G}_k = \bar{\boldsymbol{G}}\cdot\boldsymbol{E}_k$, where $\boldsymbol{E}_k$ are Cartesian unit vectors (in the undeformed configuration).

For pre-computed local deformation $\boldsymbol{F}\{\bar{\boldsymbol{F}}\}$, the sensitivity fields $\hat{\mu}^{(k)} \in \mathbb{M}_{\square}$ together with the associated Lagrange multipliers $(\hat{\lambda}^{(k)}, \hat{\bar{\lambda}}^{(k)}) \in \mathbb{L}^{\mu}_{\square}\times\mathbb{R}$ solve the problem

$$\begin{aligned}
&\frac{1}{|\Omega_{\square}|}\int_{\Omega_{\square,\mathrm{E}}} \boldsymbol{\nabla}_X\delta\mu\cdot\boldsymbol{M}\cdot\boldsymbol{\nabla}_X\hat{\mu}^{(k)}\,\mathrm{d}\Omega + \frac{1}{|\Omega_{\square}|}\int_{\Gamma^+_{\square,\mathrm{E}}} [\![\delta\mu]\!]_{\square}\,\hat{\lambda}^{(k)}\,\mathrm{d}\Gamma \\
&+\left[\frac{1}{|\Omega_{\square}|}\int_{\Omega_{\square,\mathrm{E}}}\delta\mu\,\mathrm{d}\Omega\right]\hat{\bar{\lambda}}^{(k)} = -\left[\frac{1}{|\Omega_{\square}|}\int_{\Omega_{\square,\mathrm{E}}}\boldsymbol{\nabla}_X\delta\mu\cdot\boldsymbol{M}\,\mathrm{d}\Omega\right]\cdot\bar{\boldsymbol{E}}_k \\
&\qquad\qquad \forall\delta\mu\in\mathbb{M}_{\square}, \qquad (23a)\\
&\frac{1}{|\Omega_{\square}|}\int_{\Gamma^+_{\square,\mathrm{E}}}\delta\lambda\,[\![\hat{\mu}^{(k)}]\!]_{\square}\,\mathrm{d}\Gamma = 0 \\
&\qquad\qquad \forall\delta\lambda\in\mathbb{L}^{\mu}_{\square}, \qquad (23b)\\
&\delta\bar{\lambda}\cdot\left[\frac{1}{|\Omega_{\square}|}\int_{\Omega_{\square,\mathrm{E}}}\hat{\mu}^{(k)}\,\mathrm{d}\Omega\right] = 0 \\
&\qquad\qquad \forall\delta\bar{\lambda}\in\mathbb{R}. \qquad (23c)
\end{aligned}$$

Now, upon inserting (19) into (14b), we obtain

$$\bar{\boldsymbol{J}} = \phi_0\,\langle\boldsymbol{J}\rangle_{\square,\mathrm{E}} = -\bar{\boldsymbol{M}}\cdot\bar{\boldsymbol{G}}, \tag{24}$$

where

$$\bar{\boldsymbol{M}} = \underbrace{\int_{\Omega_{\square,\mathrm{E}}}\boldsymbol{M}\,\mathrm{d}\Omega}_{:=\bar{\boldsymbol{M}}^{\mathrm{V}}} + \underbrace{\sum_{k=1}^{3}\left[\frac{1}{|\Omega_{\square}|}\int_{\Omega_{\square,\mathrm{E}}}\boldsymbol{M}\cdot\boldsymbol{\nabla}_X\hat{\mu}^{(k)}\,\mathrm{d}\Omega\right]\otimes\boldsymbol{E}_k}_{:=\Delta\bar{\boldsymbol{M}}}. \tag{25}$$

Obviously, $\bar{\boldsymbol{M}}^{\mathrm{V}}$ is the (Voigt-type) averaged mobility that ignores the effect of fluctuations. Since $\boldsymbol{M}$ is symmetrical, it is clear that $\bar{\boldsymbol{M}}^{\mathrm{V}}$ is symmetrical. However, the symmetry property of the fluctuation part $\Delta\bar{\boldsymbol{M}}$ is not obvious. To show that, indeed, $\bar{\boldsymbol{M}}$ is symmetrical, we proceed as follows: Setting $\delta\hat{\mu} = \hat{\mu}^{(l)}$ in (23a), $\delta\lambda = \hat{\lambda}^{(l)}$ in (23b) and $\delta\bar{\lambda} = \hat{\bar{\lambda}}^{(l)}$ in (23c) and eliminating, we end up with the following identity from (23a)

$$\left[\frac{1}{|\Omega_{\square}|}\int_{\Omega_{\square,\mathrm{E}}}\boldsymbol{M}\cdot\boldsymbol{\nabla}_X\hat{\mu}^{(l)}\,\mathrm{d}\Omega\right]\cdot\boldsymbol{E}_k = -\frac{1}{|\Omega_{\square}|}\int_{\Omega_{\square,\mathrm{E}}}\boldsymbol{\nabla}_X\hat{\mu}^{(l)}\cdot\boldsymbol{M}\cdot\boldsymbol{\nabla}_X\hat{\mu}^{(k)}\,\mathrm{d}\Omega. \tag{26}$$

However, by combining (25) and (26), we conclude that

$$\begin{aligned}
(\Delta\bar{\boldsymbol{M}})_{ij} &= \boldsymbol{E}_i\cdot\sum_{k=1}^{3}\left[\frac{1}{|\Omega_{\square}|}\int_{\Omega_{\square,\mathrm{E}}}\boldsymbol{M}\cdot\boldsymbol{\nabla}_X\hat{\mu}^{(k)}\,\mathrm{d}\Omega\right]\otimes\underbrace{\boldsymbol{E}_k\cdot\boldsymbol{E}_j}_{=\delta_{kj}} \\
&= \left[\frac{1}{|\Omega_{\square}|}\int_{\Omega_{\square,\mathrm{E}}}\boldsymbol{M}\cdot\boldsymbol{\nabla}_X\hat{\mu}^{(j)}\,\mathrm{d}\Omega\right]\cdot\boldsymbol{E}_i \\
&= -\frac{1}{|\Omega_{\square}|}\int_{\Omega_{\square,\mathrm{E}}}\boldsymbol{\nabla}_X\hat{\mu}^{(i)}\cdot\boldsymbol{M}\cdot\boldsymbol{\nabla}_X\hat{\mu}^{(j)}\,\mathrm{d}\Omega,
\end{aligned} \tag{27}$$

where the last identity follows from (26). In conclusion

$$(\bar{\boldsymbol{M}})_{ij} = (\bar{\boldsymbol{M}}^{\mathrm{V}})_{ij} - \frac{1}{|\Omega_{\square}|}\int_{\Omega_{\square,\mathrm{E}}}\boldsymbol{\nabla}_X\hat{\mu}^{(i)}\cdot\boldsymbol{M}\cdot\boldsymbol{\nabla}_X\hat{\mu}^{(j)}\,\mathrm{d}\Omega, \tag{28}$$

which shows the complete symmetry of $\bar{\boldsymbol{M}}$.

For a coupled boundary value problem, it is natural to consider the undeformed format of the transport problem in (13b). However, we may also push-forward to derive the equivalent of (15b) in the deformed configuration

$$-\bar{\boldsymbol{j}}\cdot\boldsymbol{\nabla} = 0 \text{ in } \bar{\omega}. \tag{29}$$

For this problem, we consider $\bar{\mu} = \bar{\mu}(\boldsymbol{x})$, and the effective flux $\bar{\boldsymbol{j}}$ is given as

$$\bar{\boldsymbol{j}} = -\bar{\boldsymbol{m}}\{\bar{\boldsymbol{F}}\}\cdot\bar{\boldsymbol{g}}, \quad \bar{\boldsymbol{g}} = \bar{\boldsymbol{F}}^{-T}\cdot\bar{\boldsymbol{G}} = \boldsymbol{\nabla}\bar{\mu}, \tag{30}$$

with

$$\bar{\boldsymbol{m}}\{\bar{\boldsymbol{F}}\} = \frac{1}{\bar{J}}\bar{\boldsymbol{F}}\cdot\bar{\boldsymbol{M}}\{\bar{\boldsymbol{F}}\}\cdot\bar{\boldsymbol{F}}^{T}, \tag{31}$$

where $\bar{\boldsymbol{m}}\{\bar{\boldsymbol{F}}\}$ is the deformation-dependent effective mobility in the deformed configuration. It is noted that $\bar{\boldsymbol{m}}$ is symmetrical since $\bar{\boldsymbol{M}}$ is symmetrical.

3.4. RVE compression test with uniaxial stress state

We shall now consider mixed control of the mechanical problem, pertinent to the virtual compression test in z-direction in Section 4. To this end, we restate (16) for the special case that we parametrize the load in $\bar{F}_{33}$ while setting $\bar{F}_{12} = \bar{F}_{23} = \bar{F}_{31} = \bar{F}_{13} = \bar{F}_{21} = \bar{F}_{32} = 0$ and $\bar{P}_{11} = \bar{P}_{22} = 0$.

As a first step, we revisit the decomposition in (11a) and seek to solve for the (sub-scale) fluctuation $\boldsymbol{u}^{\mathrm{S}}$. The macro-scale part of the displacement field becomes[5]

$$\boldsymbol{u}^{\mathrm{M}} = \hat{\boldsymbol{F}}(\bar{F}_{11},\bar{F}_{22},\bar{F}_{33})\cdot[\boldsymbol{X}-\bar{\boldsymbol{X}}], \tag{32}$$

where we introduce the expression $\hat{\boldsymbol{F}}(\bar{F}_{11},\bar{F}_{22},\bar{F}_{33}) = \sum_{i=1}^{3}\bar{F}_{ii}\boldsymbol{E}_i\otimes\boldsymbol{E}_i$ for the diagonal deformation gradient. Here, $\bar{F}_{11}$ and $\bar{F}_{22}$ become global unknowns.

The RVE problem can now be stated as: Find $(\boldsymbol{u}^{\mathrm{S}}\{\bar{F}_{33}\}, \bar{F}_{11}\{\bar{F}_{33}\}, \bar{F}_{22}\{\bar{F}_{33}\}) = (\boldsymbol{u}^{\mathrm{S}}, \bar{F}_{11}, \bar{F}_{22}) \in \mathbb{U}_0\times\mathbb{R}\times\mathbb{R}$, and $(\lambda,\bar{\lambda}) \in \mathbb{L}^{u}_{\square}\times\mathbb{R}^3$ that solves

$$\begin{aligned}
&\frac{1}{|\Omega_{\square}|}\int_{\Omega_{\square}}\boldsymbol{P}(\hat{\boldsymbol{F}}(\bar{F}_{11},\bar{F}_{22},\bar{F}_{33}) + \boldsymbol{u}^{\mathrm{S}}\otimes\boldsymbol{\nabla}_X) : [\delta\boldsymbol{u}^{\mathrm{S}}\otimes\boldsymbol{\nabla}_X]\,\mathrm{d}\Omega \\
&-\frac{1}{|\Omega_{\square}|}\int_{\Gamma^+_{\square}}\lambda\cdot[\![\delta\boldsymbol{u}^{\mathrm{S}}]\!]_{\square}\,\mathrm{d}\Gamma - \bar{\lambda}\cdot\left[\frac{1}{|\Omega_{\square}|}\int_{\Omega_{\square}}\delta\boldsymbol{u}^{\mathrm{S}}\,\mathrm{d}\Omega\right] = 0
\end{aligned}$$

[5] We note that the solution is invariant to an arbitrary translation $\bar{\boldsymbol{u}}$, which is omitted here.

$$\forall \delta \boldsymbol{u}^{\mathrm{S}} \in \mathbb{U}_{\square}, \quad (33a)$$

$$\delta \bar{F}_{11} \frac{1}{|\Omega_{\square}|} \int_{\Omega_{\square}} \underbrace{\boldsymbol{P}(\hat{\boldsymbol{F}}(\bar{F}_{11}, \bar{F}_{22}, \bar{F}_{33}) + \boldsymbol{u}^{\mathrm{S}} \otimes \boldsymbol{\nabla}_X) : [\boldsymbol{E}_1 \otimes \boldsymbol{E}_1]}_{P_{11}} \, \mathrm{d}\Omega = 0$$

$$\forall \delta \bar{F}_{11} \in \mathbb{R}, \quad (33b)$$

$$\delta \bar{F}_{22} \frac{1}{|\Omega_{\square}|} \int_{\Omega_{\square}} \underbrace{\boldsymbol{P}(\hat{\boldsymbol{F}}(\bar{F}_{11}, \bar{F}_{22}, \bar{F}_{33}) + \boldsymbol{u}^{\mathrm{S}} \otimes \boldsymbol{\nabla}_X) : [\boldsymbol{E}_2 \otimes \boldsymbol{E}_2]}_{P_{22}} \, \mathrm{d}\Omega = 0$$

$$\forall \delta \bar{F}_{22} \in \mathbb{R}, \quad (33c)$$

$$-\frac{1}{|\Omega_{\square}|} \int_{\Gamma^{+}_{\square}} \delta \boldsymbol{\lambda} \cdot [\![\boldsymbol{u}^{\mathrm{S}}]\!]_{\square} \, \mathrm{d}\Gamma = 0$$

$$\forall \delta \boldsymbol{\lambda} \in \mathbb{L}^{u}_{\square}, \quad (33d)$$

$$-\delta \bar{\boldsymbol{\lambda}} \cdot \left[\frac{1}{|\Omega_{\square}|} \int_{\Omega_{\square}} \boldsymbol{u}^{\mathrm{S}} \, \mathrm{d}\Omega \right] = 0$$

$$\forall \delta \bar{\boldsymbol{\lambda}} \in \mathbb{R}^3. \quad (33e)$$

As a result, the macroscopic deformation gradient becomes $\bar{\boldsymbol{F}}\{\bar{F}_{33}\} = \hat{\boldsymbol{F}}(\bar{F}_{11}\{\bar{F}_{33}\}, \bar{F}_{22}\{\bar{F}_{33}\}, \bar{F}_{33})$, and the local deformation gradient needed for the subsequent diffusion problem in (17) becomes

$$\boldsymbol{F}\{\bar{\boldsymbol{F}}\{\bar{F}_{33}\}\} = \bar{\boldsymbol{F}}\{\bar{F}_{33}\} + \boldsymbol{u}^{\mathrm{S}}\{\bar{F}_{33}\} \otimes \boldsymbol{\nabla}_X. \quad (34)$$

4. Diffusion in SBE subjected to compression

In this paper, it is assumed that the intrinsic fine-scale material parameters are unknown. Instead, we calibrate the RVE material model using experimental macro-scale data. Experiments on measuring elastic parameters for the SBE report $\bar{E} = 412.47$ MPa and $\bar{\nu} = 0.34$ (Tavano et al., 2024). Using these two parameters, we aim to fit the fine-scale Neo-Hooke model by minimizing the difference between an elasticity tensor with assumed isotropy and the homogenized elasticity tensor from solving the actual RVE. However, the experimental measurements are based on an SBE sample with an initial porosity of approximately 37% (Duan et al., 2023). In order to keep the calibration consistent, an RVE with approximately 37% porosity is numerically generated according to Tu et al. (2020). The RVE length is estimated to be ca. 500 nm, which is motivated by the fact that the SBE pores are reported to be between 50–200 nm (Ihrner et al., 2017; Schneider et al., 2019). The chosen RVE can be seen in Fig. 2(a).

The assumed isotropic effective elasticity tensor $\bar{\mathbf{E}}_{\mathrm{iso}}$ (for experimental data) takes the form

$$\bar{\mathbf{E}}_{\mathrm{iso}} = \frac{\bar{E}}{1+\bar{\nu}} \mathbf{I}^{\mathrm{sym}} + \frac{\bar{E}\bar{\nu}}{(1+\bar{\nu})(1-2\bar{\nu})} \boldsymbol{I} \otimes \boldsymbol{I}, \quad (35)$$

where $\mathbf{I}^{\mathrm{sym}}$ is the symmetric 4th order identity tensor. The effective elasticity tensor from solving the RVE is denoted $\bar{\mathbf{E}}_{\square}$. Clearly, unless the RVE is very large, one can expect certain degree of anisotropy in the effective elasticity tensor $\bar{\mathbf{E}}_{\square}$ due to the heterogeneity in the RVE geometry. The computation of $\bar{\mathbf{E}}_{\square}$ consists of a series of numerical perturbations around the small strain regime $\bar{\boldsymbol{F}} = \boldsymbol{I}$, i.e.

$$\bar{\mathbf{E}}_{\square} = \left. \frac{\partial \bar{\boldsymbol{P}}}{\partial \bar{\boldsymbol{F}}} \right|_{\bar{F}=I}. \quad (36)$$

The calibration is achieved upon minimizing the following objective function

$$(E, \nu) = \arg\min_{E,\nu} \|\bar{\mathbf{E}}_{\mathrm{iso}} - \bar{\mathbf{E}}_{\square}\|_{\mathrm{F}}, \quad (37)$$

where $\bar{\mathbf{E}}_{\mathrm{iso}} = \bar{\mathbf{E}}_{\mathrm{iso}}(\bar{E}, \bar{\nu})$ is known. Here, $\| \bullet \|_{\mathrm{F}}$ is the Frobenius norm. Now, since the elastic properties are assumed homogeneous on the fine-scale, only the values of the two parameters (E, ν) are unknown. The optimal values for the solid skeleton turn out to be $E = 1018.5$ MPa and $\nu = 0.44$. As a matter of convenience, the liquid electrolyte domain was modeled with a (small) fictitious stiffness of only 0.1% of the solid stiffness (where $\nu = 0.44$).

Regarding the periodic boundary conditions, they are enforced strongly in the discrete problem. This represents a special case of the weakly periodic boundary conditions[6] and simplifies for the numerical computations.

We are, finally, in the position to simulate the SBE in compression. The RVE is discretized into 53 305 tetrahedral elements (cf. Fig. 2(b)) with quadratic shape functions, resulting in a system consisting of 224 822 DOFs for the structural analysis. The maximum compression of the macro-strain from prolongation is set to 20% in the vertical z-direction. Due to the non-linear material response of Neo-Hooke, a total of 500 load steps were necessary to guarantee convergence for the considered mesh size. The deformations in the solid and liquid phases are shown in Fig. 3; the plot also shows the hydrostatic stress and relative volume change for the solid phase and liquid phase, respectively. Due to the low stiffness of the fictitious pore domain, it can be seen that some areas of the RVE are heavily compressed, see Fig. 4.

In the next step, we solve the diffusion equation while accounting for compressive loads that deform the pore channels. For the same mesh size and shape function order, the equation system consists of 37 411 DOFs for stationary diffusion. This system is solved for all values of $\bar{\boldsymbol{F}}$ used for the 500 load steps in the structural analysis, see Fig. 3(b).

Fig. 5(a) shows the effective (1st Piola–Kirchhoff) stress components as functions of prescribed macro-strain. The stress components $\bar{P}_{11}$ and $\bar{P}_{22}$ are zero as expected; the simulated compression test mimics uniaxial stress state in the effective medium. At 20% compressive macro-strain, the stress component $\bar{P}_{33}$ reaches approximately -90 MPa, which is almost three times higher than the reported compressive strength of 32.66 MPa (at 28% compressive strain) for SBEs (Tavano et al., 2024). The overestimated mechanical response can most likely be attributed to the choice of (over)simplified constitutive material model; i.e., the lack of consideration for inelastic and fracture processes.

Fig. 5(b) shows how the pore volume fraction changes from the initial 37% to approximately 30% at the final stage of the compression; this volume fraction change corresponds to a volume reduction of approximately 19%. Here, the deformed pore volume fraction $\boldsymbol{\Phi}$ is defined as the current (deformed) pore volume divided by the undeformed microstructure volume.

It can be observed in Fig. 6(a) that the normalized effective mobility component $\frac{\bar{M}_{11}}{m}$, which is orthogonal to the compression direction, is reduced by approximately 26% for a compression of 20%. Here, m is the isotropic fine-scale mobility.[7] It is intuitive that the compression of the SBE leads to a reduction in pore volume, thereby impeding the ion transport. Additionally, the plot also shows $\frac{\bar{M}_{22}}{m}$, which is also orthogonal to the compression direction. The normalized effective mobility components at 20% macroscopic strain are $\frac{\bar{M}_{11}}{m} = 0.085$ and $\frac{\bar{M}_{22}}{m} = 0.105$. This indicates that the chosen RVE has some apparent anisotropy, meaning that the RVE size is not sufficiently large to be fully representative. For completeness, Fig. 6(b) shows the effective mobility components in the deformed configuration.

Fig. 7 shows multiple curves with different values of the fictitious elasticity modulus of the pore space. The investigation confirms that assigning 0.1% of the solid's elasticity modulus to the pore space leads to a converged solution; i.e., there is nothing to gain by decreasing the fictitious stiffness further.

[6] Note that the original problem was stated using weakly periodic boundary conditions for generality and because the constraints become more convenient to state.

[7] The fine-scale mobility m is treated as a known property for the liquid electrolyte. No number on m is presented here since the framework is valid for any choice of m. Additionally, the final results are more useful in normalized format.

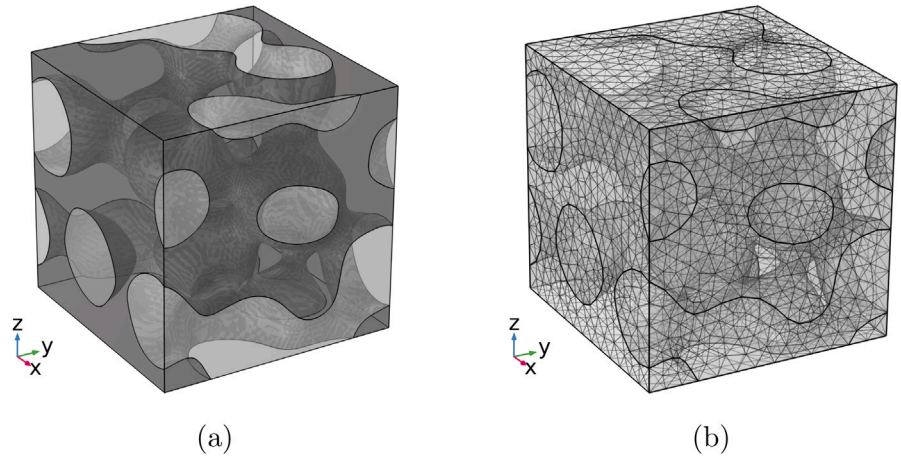

Fig. 2. Initial undeformed RVE domain in (a), and corresponding mesh in (b). RVE side length is chosen to be 500 nm as each pore is assumed to be between 50–200 nm in diameter. The solid polymer is highlighted in dark gray, while the liquid electrolyte is highlighted in light gray. The chosen RVE is a randomly generated microstructure of the "trabecular" type according to Tu et al. (2020).

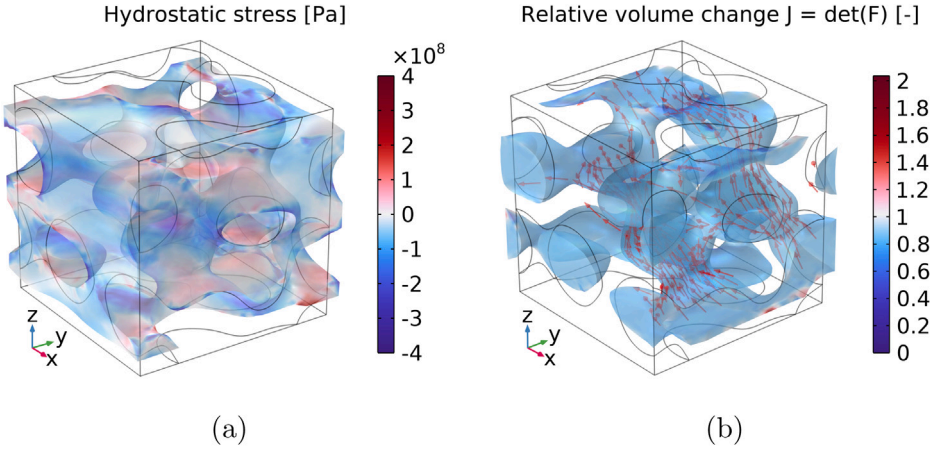

Fig. 3. The plot shows (a) hydrostatic stress in deformed solid skeleton, and (b) deformed state of the pore space Ω_E with arrows showing the diffusion path. A few local stress concentrations (magnitude ca. 2.3 GPa) are filtered out from (a) to provide a better visualization of the stress distribution.

Fig. 4. Zooming into significantly compressed areas of the pore space (marked in blue) where the determinant of the deformation gradient $J < 0.01$ is very small.

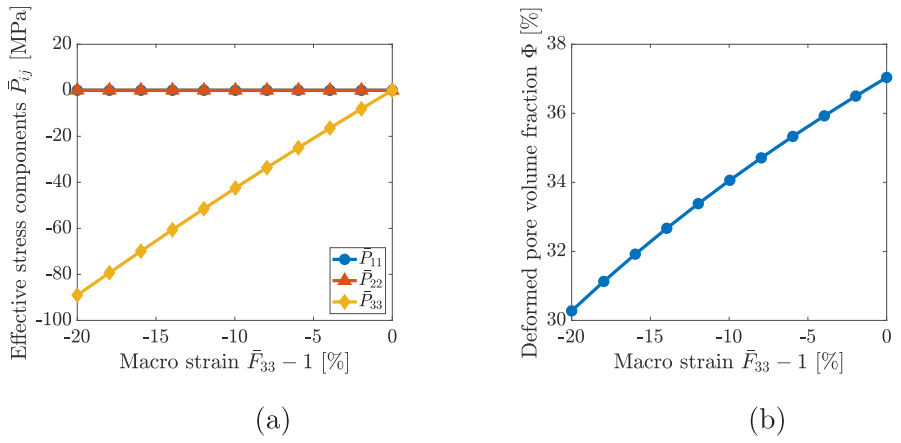

Fig. 5. Mechanical response; (a) effective 1st Piola–Kirchhoff stress, and (b) deformed pore volume fraction $\boldsymbol{\Phi} = \phi_0 \langle J \rangle_{\square,\mathrm{E}}$ of the RVE.

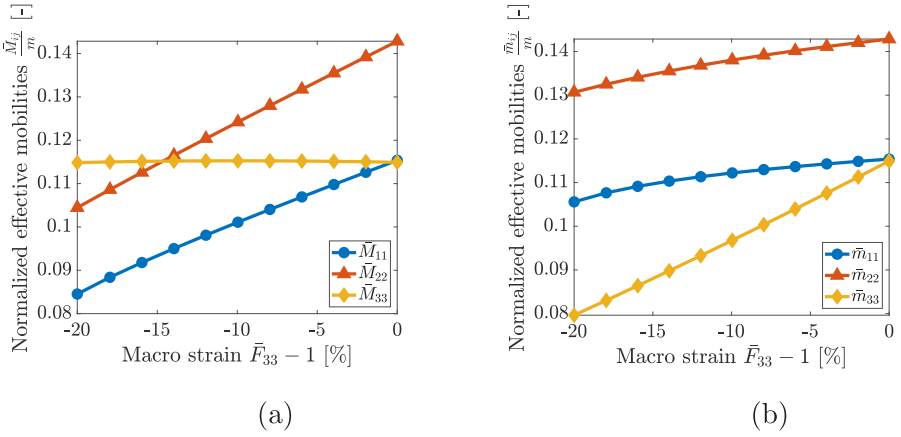

Fig. 6. Components of the effective (normalized) mobility tensor in (a) undeformed configuration, and (b) deformed configuration, where m is the isotropic fine-scale mobility. Note that all curves would have the same starting point at $\bar{F}_{33} - 1 = 0$ if the RVE was representative.

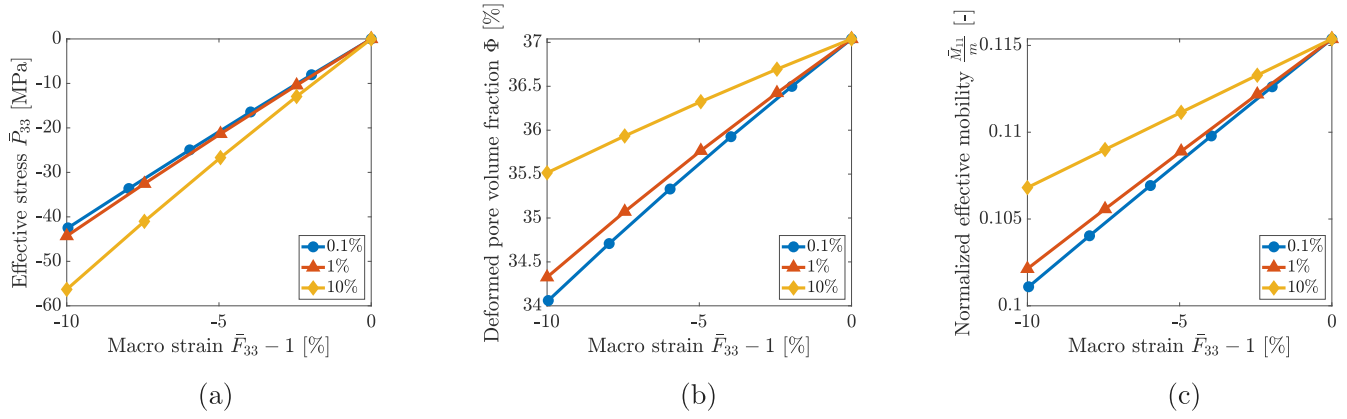

Fig. 7. Parametric study on the influence of the fictitious stiffness in the pore domain; (a) effective stress $\bar{P}_{33}$, (b) deformed pore volume fraction $\boldsymbol{\Phi} = \phi_0 \langle J \rangle_{\square,\mathrm{E}}$ of the RVE, and (c) effective (normalized) mobility $\frac{\bar{M}_{11}}{m}$, where m is the isotropic fine-scale mobility.

5. Conclusions

In this paper, we have developed a framework for computing the deformation-dependent effective mobility for the Structural Battery Electrolyte. The structural analysis assumes finite strains and a compressible Neo-Hooke material model, which was calibrated based on experimental values of the effective parameters $(\bar{E}, \bar{\nu})$. Stationary diffusion was employed using mass balance and constitutive relation of Fickian type. The pore volume reduction due to compressive loads was taken into consideration. Fig. 6(a) shows that the normalized effective mobility component $\frac{\bar{M}_{11}}{m}$ was reduced by 26% due to a 20% macroscopic (strain) compression of the considered bicontinuous SBE with 37% initial porosity.

In the mechanical analysis, the pore space was modeled as a solid with a small artificial stiffness. In this way, the deformation gradient $\boldsymbol{F}$ could be computed for the pore space, which was used to establish the ionic Piola-flux. Moreover, this method also prevents penetration of contacting pore surfaces by requiring the local pore volume to be

positive, i.e., $J > 0$. However, the issue with this method is that the pore space will exhibit artificial elastic properties (increased stiffness), which in turn affects the overall deformation of the SBE. This effect is unwanted if the goal is to simulate the response of a fully drained SBE. Indeed, the assumption of a drained SBE provides the upper bound for the homogenized compliance due to the lack of resistance and pressure build-up during redistribution of the liquid inside the pores.

A way to circumvent the artificial stiffness in the liquid phase would be to either (i) re-mesh the pore space domain according to the displacements, or (ii) introduce a fictitious elastic solid in the pores that will deform, but not give rise to any reaction forces that might affect the solid phase. However, such a procedure would still need to be complemented with a proper contact formulation to avoid the risk of self-penetration.

In view of the calibration, it is vital to conduct a validation study to evaluate the usefulness of the compressible Neo-Hooke material model. Most likely, there are other viable alternatives that are potentially more suitable for compression of SBE. All things considered, this paper represents a starting point for the more complete analysis of electro-chemically coupled deformation-dependent ionic transport.

CRediT authorship contribution statement

Vinh Tu: Writing – review & editing, Writing – original draft, Visualization, Validation, Software, Methodology, Investigation, Formal analysis, Data curation, Conceptualization. **Fredrik Larsson:** Writing – review & editing, Supervision, Methodology, Funding acquisition, Conceptualization. **Kenneth Runesson:** Writing – review & editing, Supervision, Methodology, Funding acquisition, Conceptualization. **Ralf Jänicke:** Writing – review & editing, Supervision, Methodology, Funding acquisition, Conceptualization.

Declaration of competing interest

The authors declare that they have no known competing financial interests or personal relationships that could have appeared to influence the work reported in this paper.

Acknowledgments

This research was funded by the Swedish Research Council (VR), Sweden via the grants No. 2017-05192, No. 2019-05080 and No. 2020-05057. Furthermore, funding was also received from the USAF EOARD, USA (Award No. FA8655-21-1-7038). All are gratefully acknowledged.

Data availability

No data was used for the research described in the article.

References

Asp, L.E., Greenhalgh, E.S., 2014. Structural power composites. Compos. Sci. Technol. 101, 41–61.

Asp, L.E., Johansson, M., Lindbergh, G., Xu, J., Zenkert, D., 2019. Structural battery composites: a review. Funct. Compos. Struct. 1 (4), 042001.

Bharali, R., Larsson, F., Jänicke, R., 2021. Computational homogenisation of phase-field fracture. Eur. J. Mech. A Solids 88, 104247.

Bonet, J., Wood, R.D., 2008. Nonlinear Continuum Mechanics for Finite Element Analysis, second edition Cambridge University Press.

Börjesson, E., Larsson, F., Runesson, K., Remmers, J.J., Fagerström, M., 2023. Variationally consistent homogenisation of plates. Comput. Methods Appl. Mech. Engrg. 413, 116094.

Carlstedt, D., Runesson, K., Larsson, F., Tu, V., Jänicke, R., Asp, L.E., 2022. Computational modelling of structural batteries accounting for stress-assisted convection in the electrolyte. Int. J. Solids Struct. 238, 111343.

Duan, S., Cattaruzza, M., Tu, V., Auenhammer, R.M., Jänicke, R., Johansson, M.K., Liu, F., Asp, L.E., 2023. Three-dimensional reconstruction and computational analysis of a structural battery composite electrolyte. Commun. Mater. 4 (1), 49.

Geers, M., Kouznetsova, V., Brekelmans, W., 2010. Multi-scale computational homogenization: Trends and challenges. J. Comput. Appl. Math. 234 (7), 2175–2182, Fourth International Conference on Advanced COmputational Methods in ENgineering (ACOMEN 2008).

Griffiths, E., Wilmers, J., Bargmann, S., Reddy, B.D., 2020. Nanoporous metal based composites: Giving polymers strength and making metals move. J. Mech. Phys. Solids 137, 103848.

Griso, G., Rohan, E., 2007. On the homogenization of a diffusion–deformation problem in strongly heterogeneous media. Ric. di Mat. 56, 161–188.

Hill, R., 1963. Elastic properties of reinforced solids: Some theoretical principles. J. Mech. Phys. Solids 11 (5), 357–372.

Ihrner, N., Johannisson, W., Sieland, F., Zenkert, D., Johansson, M., 2017. Structural lithium ion battery electrolytes via reaction induced phase-separation. J. Mater. Chem. A 5, 25652–25659.

Johannisson, W., Zenkert, D., Lindbergh, G., 2019. Model of a structural battery and its potential for system level mass savings. Multifunct. Mater. 2 (3), 035002.

Kaessmair, S., Steinmann, P., 2018. Computational first-order homogenization in chemo-mechanics. Arch. Appl. Mech. 88, 271–286.

Klepach, D., Zohdi, T., 2014. Strain assisted diffusion: Modeling and simulation of deformation-dependent diffusion in composite media. Compos. Part B: Eng. 56, 413–423.

Kouznetsova, V., Brekelmans, W., Baaijens, F., 2001. An approach to micro-macro modeling of heterogeneous materials. Comput. Mech. 27, 37–48.

Kouznetsova, V., Geers, M., Brekelmans, W., 2004. Multi-scale second-order computational homogenization of multi-phase materials: a nested finite element solution strategy. Comput. Methods Appl. Mech. Engrg. 193 (48), 5525–5550, Advances in Computational Plasticity.

Larsson, F., Runesson, K., Saroukhani, S., Vafadari, R., 2011. Computational homogenization based on a weak format of micro-periodicity for RVE-problems. Comput. Methods Appl. Mech. Engrg. 200 (1), 11–26.

Larsson, F., Runesson, K., Su, F., 2010. Variationally consistent computational homogenization of transient heat flow. Internat. J. Numer. Methods Engrg. 81 (13), 1659–1686.

Michel, J., Moulinec, H., Suquet, P., 1999. Effective properties of composite materials with periodic microstructure: a computational approach. Comput. Methods Appl. Mech. Engrg. 172 (1), 109–143.

Miehe, C., Koch, A., 2002. Computational micro-to-macro transitions of discretized microstructures undergoing small strains. Arch. Appl. Mech. 72, 300–317.

Miehe, C., Schröder, J., Schotte, J., 1999. Computational homogenization analysis in finite plasticity simulation of texture development in polycrystalline materials. Comput. Methods Appl. Mech. Engrg. 171 (3), 387–418.

Nemat-Nasser, S., Hori, M., 2013. Micromechanics: Overall Properties of Heterogeneous Materials. Elsevier.

Polukhov, E., Keip, M.-A., 2020. Computational homogenization of transient chemo-mechanical processes based on a variational minimization principle. Adv. Model. Simul. Eng. Sci. 7, 1–26.

Rohan, E., Cimrman, R., 2012. Multiscale FE simulation of diffusion-deformation processes in homogenized dual-porous media. Math. Comput. Simulation 82 (10), 1744–1772, "The Fourth IMACS Conference : Mathematical Modelling and Computational Methods in Applied Sciences and Engineering" Devoted to Owe Axelsson in ocassion of his 75th birthday.

Rollin, D., Larsson, F., Runesson, K., Jänicke, R., 2023. Upscaling of chemo-mechanical properties of battery electrode material. Int. J. Solids Struct. 281, 112405.

Schneider, L.M., Ihrner, N., Zenkert, D., Johansson, M., 2019. Bicontinuous electrolytes via thermally initiated polymerization for structural lithium ion batteries. ACS Appl. Energy Mater. 2 (6), 4362–4369.

Shirshova, N., Johansson, P., Marczewski, M.J., Kot, E., Ensling, D., Bismarck, A., Steinke, J.H.G., 2013. Polymerised high internal phase ionic liquid-in-oil emulsions as potential separators for lithium ion batteries. J. Mater. Chem. A 1, 9612–9619.

Tavano, R., Spagnol, M., Al-Ramahi, N., Joffe, R., Xu, J., Asp, L.E., 2024. Mechanical characterisation of a structural battery electrolyte. Polymer 312, 127646.

Tu, V., Asp, L.E., Shirshova, N., Larsson, F., Runesson, K., Jänicke, R., 2020. Performance of bicontinuous structural electrolytes. Multifunct. Mater. 3 (2), 025001.

Tu, V., Larsson, F., Runesson, K., Jänicke, R., 2023. Variationally consistent homogenization of electrochemical ion transport in a porous structural battery electrolyte. Eur. J. Mech. A Solids 98, 104901.

Voges, J., Duvigneau, F., Juhre, D., 2022. On the deformation dependency of the diffusion flux in solids at large deformations. Contin. Mech. Thermodyn. 34, 829–839.

Waseem, A., Heuzé, T., Stainier, L., Geers, M., Kouznetsova, V., 2020. Enriched continuum for multi-scale transient diffusion coupled to mechanics. Adv. Model. Simul. Eng. Sci. 7, 14.

Yvonnet, J., Computational Homogenization of Heterogeneous Materials with Finite Elements, vol. 258, Springer.

Zohdi, T.I., Wriggers, P., 2008. An Introduction to Computational Micromechanics. Springer Science & Business Media.